The effect of density ratio on a downslope gravity current

Bruce Balderrama

June 2019

The physics of a downslope gravity current, for various density ratios, moving into a two-layer stratified ambient is analyzed. Direct numerical simulations are conducted using the code PARTIES (PARTicleladen flows via immersed boundarIES), which is a three-dimensional Navier-Stokes solver coupled to an interface-resolving Immersed Boundary Method (IBM) for fully resolved particle-fluid simulations. This project focuses solely on fluid flow and does not include particles. When the gravity current is lighter than the lower layer of the ambient fluid, the gravity current is observed to intrude at the pynocline, or layer where the density gradient is the greatest. In addition, when the gravity current is heavier than the lower layer, it splits into an intrusion at the pynocline and a hyperpycnal current descending beneath the lower layer. The output data of the simulations provides physical insight into the gravity current flow, particularly the energy components of the entire fluid volume and the velocity and position of the gravity current front. When the gravity current is released, the potential energy of the current fluid is converted into kinetic energy and viscous losses accumulate. As the current pierces the pynocline, a fraction of its kinetic energy is used to lift the dense ambient fluid, so that the overall kinetic energy of the flow peaks and then steadily declines. The total energy of the system is expected to remain constant, but does not in the simulations due to an overestimation of the viscous losses, as well as an unphysical mass loss.

1 Introduction

Gravity currents appear when a fluid of one density propagates into another fluid of different density and the motion is mainly in the horizontal direction (Ungarish 2009). When a fluid is stably stratified, the displaced fluid parcel always feels a restoring force directed back to its equilibrium position and its motion is oscillatory (Sutherland 2010). As a gravity current flows, it entrains ambient water and is gradually diluted. Entrainment refers to changes in volume or density due to mixing effects (Ungarish 2009). In two-layer stratifications, a gravity current that is lighter than the lower ambient fluid will intrude at the pynocline, which is the layer where the density gradient is greatest within a body

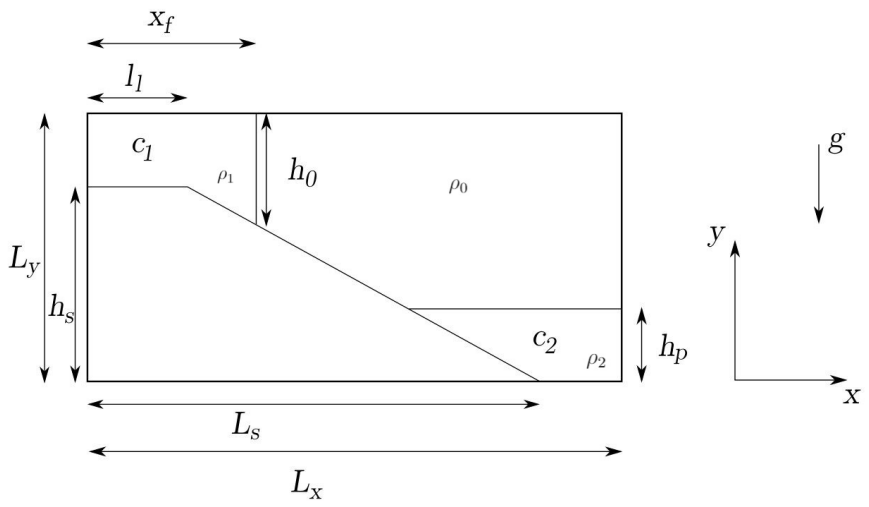

Figure 1: Initial numerical setup for analyzing the effect of density ratio $\frac{\rho_2-\rho_0}{\rho_1-\rho_0} = \frac{c_2}{c_1}$ on a downslope gravity current. The gravity current concentration is c_1 and the lower ambient concentration is c_2. At time $t = 0$, the lock is released and the gravity current begins to move down the slope.

of water. The gravity current will split into an intrusion at the pynocline and a hyperpycnal bottom current descending beneath the lower layer if it contains fluid denser than the lowest layer (Hogg et al. 2018).

In the present investigation, the flow of a downslope gravity current (for various density ratios) moving into a two-layer stratified ambient is analyzed via direct numerical simulations. Section 2 presents the flow configuration and discusses the governing equations, along with the characteristic scales. Section 3 discusses the numerical method and the simulation setup to run the PARTIES code. Section 4 lists the simulation parameters and focuses on the analysis of the flow physics, in particular the influence of density ratio on various components of the overall energy budget, the gravity current wave velocity and position, and the mass loss due to utilizing the Immersed Boundary Method (IBM). Section 5 summarizes the key discoveries and presents the conclusions of the work.

2 Governing Equations

The initial configuration of the simulations is shown in figure 1. A lock with scalar concentration c_1 is separated from the ambient by a virtual gate. The lower, denser region of the two-layer ambient has an initial scalar concentration c_2 and there is no scalar concentration in the upper ambient region. The total width of the fluid domain is given by L_x and the height by L_y. The height of the slope and length of the slope are given by h_s and L_s respectively. The

length of the lock is denoted by l_l and the initial x front location of the gravity current wave is indicated by x_f. The height of the pynocline of the two-layer ambient is specified by h_p. The height of the lock is given by h_0.

The three-dimensional Navier-Stokes equations for incompressible flows can be solved for and one can use the Boussinesq approxmation, assuming that density changes due to salt or temperature variations are small. The scalar concentration field is given by the advection-diffusion equation

$$\frac{\partial \psi}{\partial t} + \mathbf{u} \cdot \nabla \psi = \nabla \cdot (\kappa \nabla \psi) \,. \tag{1}$$

where ψ is the diffusing scalar quantity, $\mathbf{u}$ is the fluid velocity, and κ is the diffusivity coefficient. The fluid velocity vector is decomposed in Cartesian coordinates as $\mathbf{u} = u\mathbf{e_x} + v\mathbf{e_y} + w\mathbf{e_z}$. The dimensional governing equations (continuity, Navier-Stokes, and the advection-diffusion equation for the concentration fields) are given by

$$\nabla \cdot \mathbf{u} = 0 \,, \tag{2}$$

$$\frac{\partial \mathbf{u}}{\partial t} + (\mathbf{u} \cdot \nabla)\, \mathbf{u} = -\frac{1}{\rho_0} \nabla p + \nu \Delta \mathbf{u} + \frac{\rho - \rho_0}{\rho_0} \mathbf{g} \,, \tag{3}$$

$$\frac{\partial c_i}{\partial t} + \mathbf{u} \cdot \nabla c_i = \kappa_c \Delta c_i, \; i = \{c, a\} \,. \tag{4}$$

where p represents the pressure, ρ denotes the local density with the fresh water ρ_0 acting as a reference value, and c_c and c_a are the salinity concentrations of the current and ambient fluid, respectively. The kinematic viscosity of the water is assumed to be constant at $\nu = 10^{-6} m^2/s$. The influence of scalar diffusivity κ_c on the propagation velocity of a gravity current is small as long as $\kappa_c \leq \nu$, which leads to the choice of $\kappa_c = \nu$ for simplicity (Härtel, Meiburg, and Necker 2000). The gravitational acceleration is given by $\mathbf{g} = -g\mathbf{e_y}$. Density is written as a linear function of salinity such that

$$\rho = \rho_0 (1 + \alpha c_c + \alpha c_a) \,, \tag{5}$$

where $\alpha = \frac{\partial \rho}{\partial c} =$ cst. defines the expansion coefficient.

The lock height h_o is used as a reference length, since it directly affects the propagation velocity of the gravity current. The reference concentration is chosen as the initial concentration of the lock $c_c(t = 0) = c_1$. The buoyancy velocity is defined based on the initial density difference between the lock and the ambient fluid

$$u_b = \sqrt{\frac{\rho_1 - \rho_0}{\rho_0} g h_0} \,, \tag{6}$$

where $\rho_1 = \rho_0(1 + \alpha c_1)$ is the density of the gravity current fluid initially contained behind the lock and ρ_0 is the density of the upper ambient fluid

(figure 1). The reference time scale can be defined as $T = \frac{h_0}{u_b}$. The governing equations are now nondimensionalized using the definitions below.

$$\mathbf{x}^* = \frac{\mathbf{x}}{h_0}\,, \tag{7}$$

$$\mathbf{u}^* = \frac{\mathbf{u}}{u_b}\,, \tag{8}$$

$$t^* = \frac{t}{T}\,, \tag{9}$$

$$p^* = \frac{p}{\rho_0 u_b^2}\,, \tag{10}$$

$$c_i^* = \frac{c_i}{c_1},\ i = \{c, a\}\,, \tag{11}$$

$$\nabla^* = h_0 \nabla\,, \tag{12}$$

$$\Delta^* = h_0^2 \Delta\,. \tag{13}$$

The nondimensional form of the governing equations are found

$$\nabla^* \cdot \mathbf{u}^* = 0\,, \tag{14}$$

$$\frac{\partial \mathbf{u}^*}{\partial t^*} + (\mathbf{u}^* \cdot \nabla^*)\,\mathbf{u}^* = -\nabla^* p^* + \frac{1}{Re}\Delta^* \mathbf{u}^* - (c_c^* + c_a^*)\mathbf{e_y}\,, \tag{15}$$

$$\frac{\partial c_i^*}{\partial t^*} + \mathbf{u}^* \cdot \nabla^* c_i^* = \frac{1}{Pe}\Delta^* c_i^*,\ i = \{c, a\}\,. \tag{16}$$

where $Re = \frac{u_b h_0}{\nu}$ is the Reynolds number and $Pe = ReSc$ is the Peclet number, with $Sc = \frac{\nu}{\kappa_c}$ being the Schmidt number. The Schmidt number is set to unity, as defined earlier.

3 Numerical Method and Simulation Setup

The code utilized in this project is called PARTIES (PARTicleladen flows via immersed boundarIES), a three-dimensional Navier-Stokes solver coupled to an interface-resolving Immersed Boundary Method (IBM) for fully resolved particle-fluid simulations. In the present work, only fluid flow without particles will be analyzed. PARTIES was written in C and developed in lab under PhD work of Dr. Edward Biegert as well as Dr. Bernhard Vorwinckel. Additional features of PARTIES used are the result of the work of Dr. Thomas Köllner (Volume of Fluid Method and scalar transport solver) and PhD student Raphael Ouillion (active particles and periodic stratified shear).

PARTIES utilizes a staggered uniform grid in Cartesian coordinates. In the staggered grid, individual variables are defined at different gridpoints, such that pressure and concentration is defined at the center of each cell and the velocities are defined at the cell faces (Fletcher 1991). A second-order finite difference scheme is used to discretize the Navier-Stokes equations in all three

directions and a low-storage third order Runge-Kutta (RK) method is used to integrate the discretized equations in time. RK methods are classified as one-step methods, which do not use any information from previous steps and utilize intermediate approximations (Ascher and Petzold 1998). In addition, the Immersed Boundary Method is used to ensure no-slip boundary condition on the slope (M.M., Nasr-Azadani, and Meiburg 2011). IBM adds a body force $\mathbf{f}$ to the Navier-Stokes equation and advection-diffusion equation in order to impose conditions along solid boundaries. In TURBINS (**TURB**idity currents via **I**mmersed boundary **N**avier-**S**tokes simulations), a direct forcing method is used to solve directly for the forcing term $\mathbf{f}$ at a new time step. Interpolation techniques are used to enforce the boundary conditions via imposing constraints on neighboring grid nodes. In TURBINS, a condition is imposed at the first node inside the solid, not the fluid. The value of the desired variable at the mirrored fluid node is computed via interpolation. The process is discussed in more detail in M.M., Nasr-Azadani, and Meiburg 2011. A pressure projection method is used to calculate the pressure and correct the velocity field to satisfy continuity. Time stepping without particles is achieved with a low storage third order, hybrid implicit/explicit Runge-Kutta method derived by Spalart, Moser, and Rogers 1990. At time step t^n one can solve for velocity $\mathbf{u}^{n,k}$ and pressure $p^{n,k}$ with substeps k=1,2,3, where

$$\mathbf{u}^{n-1,3} := \mathbf{u}^{n,0},\ p^{n-1,3} := p^{n,0}\ . \tag{17}$$

The governing equations are first transformed into conservative form from the definition of continuity for incompressible flows, where the conservative form is defined as

$$\partial_0\,\phi + \partial_j F_j(\phi) = sources\ . \tag{18}$$

where ϕ is the conserved property of interest and $F_j(\phi)$ describes the fluxes of ϕ (Bennett 2012). The time stepping scheme in the absence of particles is given below

$$\begin{aligned} -\kappa_j\nabla^2 c_j^k + \frac{c_j^k}{\Delta t^n\alpha^k} &= \frac{c_j^{k-1}}{\Delta t^n\alpha^k} + \kappa_j\nabla^2 c_j^{k-1} \\ &-\frac{\gamma_k}{\alpha_k}\nabla\cdot(\mathbf{u}c_j)^{k-1} - \frac{\zeta_k}{\alpha_k}\nabla\cdot(\mathbf{u}c_j)^{k-2}\ , \end{aligned} \tag{19}$$

$$\begin{aligned} \frac{\mathbf{u}^* - \mathbf{u}^{n,k-1}}{\Delta t^n\alpha_k} &= \nu\nabla^2(\mathbf{u}^* + \mathbf{u}^{n,k-1}) - \frac{2}{\rho_0}\nabla p^{n,k-1} \\ -\frac{\gamma_k}{\alpha_k}\nabla\cdot(\mathbf{uu})^{n,k-1} - \frac{\zeta_k}{\alpha_k}\nabla\cdot(\mathbf{uu})^{n,k-2} &+ 2\mathbf{g}\sum_j^J \beta_j c_j^k\ , \end{aligned} \tag{20}$$

$$\nabla^2\Phi^k = \frac{\nabla\cdot\mathbf{u}^*}{2\alpha_k\Delta t^n}\ , \tag{21}$$

$$\mathbf{u}^{n,k} = \mathbf{u}^* - 2\alpha_k\Delta t\nabla\Phi\ , \tag{22}$$

$$p^{n,k} = p^{n,k-1} + \rho_0\Phi^k. \tag{23}$$

where Δt^n is the time step at iteration n and $\alpha_k = \{\frac{4}{15}\ \frac{1}{15}, \frac{1}{6}\}$, $\gamma_k = \{\frac{8}{15}\ \frac{5}{12}, \frac{3}{4}\}$, and $\zeta_k = \{0, -\frac{17}{60}, -\frac{5}{12}\}$ are the RK coefficients of substeps $k = \{1, 2, 3\}$ respectively (Spalart, Moser, and Rogers 1990). The J density-contributing scalar fields are first advanced to the next substep k using an implicit scheme, particularly the Crank-Nicolson scheme. The choice of $\zeta_1 = 0$ allows for previous substep information to be discarded when the time step n advances. This scheme utilizes the trapezoidal rule and can be regarded as an equal blend of first order explicit and implicit Euler schemes, and provides second order accuracy (Ferziger and Perić 2002). A preliminary velocity field $\mathbf{u}^*$ is calculated using Crank-Nicolson for the diffusion terms and an explicit scheme for the advection terms. The updated concentrated fields are used in the Boussinesq term. The Poisson problem for the pseudo-pressure Φ^k is solved. Following the projection step, the velocity and pressure are corrected, finalizing the substep. The general formulation for the projection method is shown in (Fletcher 1991) and (Ferziger and Perić 2002).

In order to run the code and process the results, several steps are followed for each simulation. First, the inputs to the code are determined from the nondimensionalized equations and are entered in files such as parties.inp. Sources are modified in files such as boundary.h for boundary conditions and solution methods. The make command is used to compile the sources. On a local machine, the newly created executable file could be run. However, for larger scale simulations and to run multiple simulations simultaneously, the supercomputer Stampede2 is utilized. Stampede2 is located at The University of Texas at Austin's Texas Advanced Computing Center (TACC) and features 4,200 Knights Landing (KNL) nodes and 1,736 Intel Xeon Skylake (SKX) nodes. Usage of Stampede2 is made possible via XSEDE. The Extreme Science and Engineering Discovery Environment (XSEDE) is a National Science Foundation (NSF)-funded virtual organization that integrates and coordinates usage of high-performance computing and data resources. To run the code on Stampede2, the source files had to be compiled on the Stampede2 file system using the make command. Then, a batch script is configured to specify the usage of computing nodes. PARTIES utilizes message passing interface (MPI), which is a standardized and portable message-passing standard designed for parallel computing. Once the script is prepared, a job could be queued with the sbatch command. Once the simulations are finished, the output files are generated on the Stampede2 file systems and are copied over to the local machine for post-processing. Post-processing of the .h5 files is accomplished using VisIt, an open-source visualization tool, and Matlab. Several scripts are created on Matlab to read the output files and generate plots of desired data, such as potential energy of the gravity current fluid versus time.

In the present investigation, the computational domain is discretized by $(N_x \times N_y \times N_z) = (4000 \times 300 \times 2)$ cells, corresponding to a grid size of $\frac{\Delta x}{h_o} = \frac{\Delta y}{h_o} = \frac{\Delta z}{h_o} = 0.01$. $Re = 1000$ flow is analyzed with a total simulation time $t/T = 80$. The initial flow profile was specified as zero flow. In the boundary.h file mentioned above, the boundary conditions are specified. Slip boundary

conditions are employed at the left, right, and top walls and periodic conditions are utilized in the spanwise direction. No-slip conditions are used at the bottom wall and on the slope, via the Immersed Boundary Method. In addition, the Boussinesq approximation is enabled in the source file. The width of the domain is chosen as the minimum size, 2 grid points in the z-direction, so that the simulation is pseudo-2D.

4 Results

4.1 Simulation Parameters

Sim.	c_2/c_1	L_x/h_0	L_y/h_0	L_z/h_0	l_l/h_0	x_f/h_0	L_s/h_0	h_s/h_0	h_p/h_0	Re
1	0.4	40	3	0.02	1.0	7.14	30	2.537	1.0	1,000
2	0.6	40	3	0.02	1.0	7.14	30	2.537	1.0	1,000
3	0.8	40	3	0.02	1.0	7.14	30	2.537	1.0	1,000
4	1.0	40	3	0.02	1.0	7.14	30	2.537	1.0	1,000
5	1.2	40	3	0.02	1.0	7.14	30	2.537	1.0	1,000

Table 1: Simulation parameters used to investigate the effect of density ratio on gravity current flow down a slope.

Direct numerical simulations are conducted for the dimensionless parameters illustrated in figure 1. Table 1 describes the simulations to investigate the effect of various density ratios $\frac{\rho_2-\rho_0}{\rho_1-\rho_0} = \frac{c_2}{c_1}$ on the physics of gravity current flow. All of the length dimensions are nondimensionalized by the lock height h_0.

4.2 Gravity current wave concentration, velocity, and front locations

The gravity current fluid concentration is plotted at a simulation time of $t/T = 60$ for various density ratios (figure 2). This is at a simulation time after the gravity current has hit the pynocline of the ambient fluid. When the gravity current is lighter than the lower layer ($c_2/c_1 > 1$), then the gravity current intruded at the pynocline with no hyperpycnal component. This is clearly shown in the subplot for density ratio $c_2/c_1 = 1.2$. When the gravity current is heavier than the lower layer ($c_2/c_1 < 1$), then the gravity current splits into an intrusion at the pynocline and a hyperpycnal bottom current that continues to move down the slope. This hyperpycnal component is most evident in the subplot for the density ratio $c_2/c_1 = 0.4$. As c_2/c_1 increases, the gravity current is more dominated by the intrusion component and less by the hyperpycnal component.

The x front location x_f of the gravity current wave at a particular time is the rightmost horizontal position at which

$$c_c(x, y) \geq c_t \, . \tag{24}$$

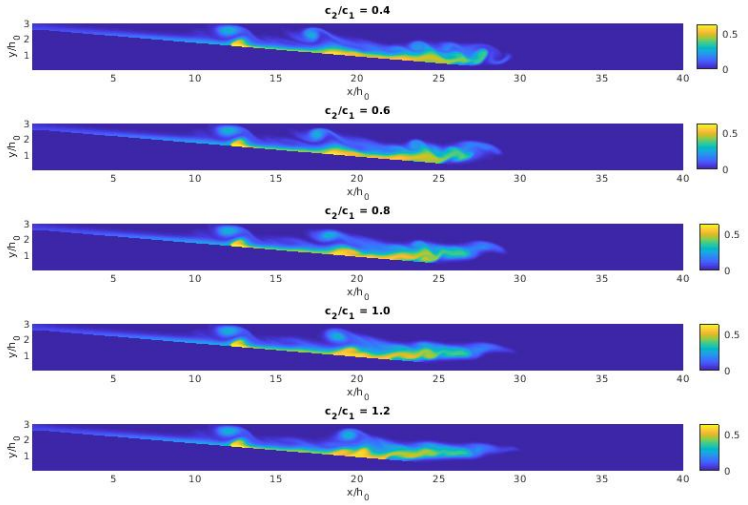

Figure 2: Snapshots of the gravity current fluid concentration c_c at $t/T = 60$ for different c_2/c_1.

where a concentration threshold $c_t = 0.05$ is chosen. The x position of the gravity current front x_f versus time for various density ratios is shown in figure 3a. As the simulation progresses, x_f increases because the gravity current is moving further down the slope. There is no clear correlation between the density ratio and x_f location. The y front location of the gravity current y_f, or the height of the gravity current wave, is defined as the y location which corresponds to the rightmost horizontal position that meets the concentration threshold. A plot of y_f as a function of time for various density ratios is shown in figure 3b. For all simulations, y_f decreases for the initial time period until $t/T = 23$. The density ratio has a clear effect on the y_f for later times. Lower density ratios result in gravity currents that descend lower before moving upwards. This reaffirms the physical expectation that the hyperpycnal component of the gravity current descends beneath the lower layer for $c_2/c_1 < 1$. For higher density ratios, there is still oscillatory movement in the wave, but the motion is more horizontal, just above the pynocline $h_p/h_0 = 1.0$. This confirms the expectation that the gravity current will intrude at the pynocline for $c_2/c_1 > 1$.

The horizontal velocity of the gravity current u_c is calculated from the derivative of the horizontal front location x_f with respect to time. The plot of u_c/u_b as a function of time for various density ratios is shown in figure 4. The maximum velocity $u_c/u_b = 0.49$, where u_b is the buoyancy velocity defined earlier, for all c_2/c_1 occurs at $t/T = 18$. The large decreases in the current velocity are a result of numerical error, such as for the density ratio $c_2/c_1 = 0.6$ at $t/T = 53.5$. The gravity current velocity increases for all density ratios during the initial period

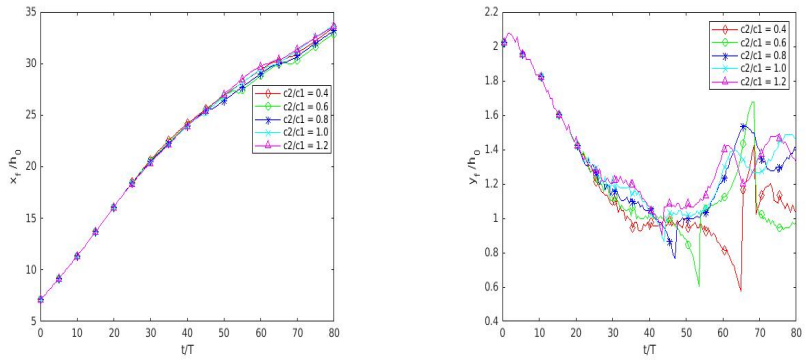

(a) The x front location x_f (b) The y front location y_f

Figure 3: Gravity current front locations as a function of time for various c_2/c_1.

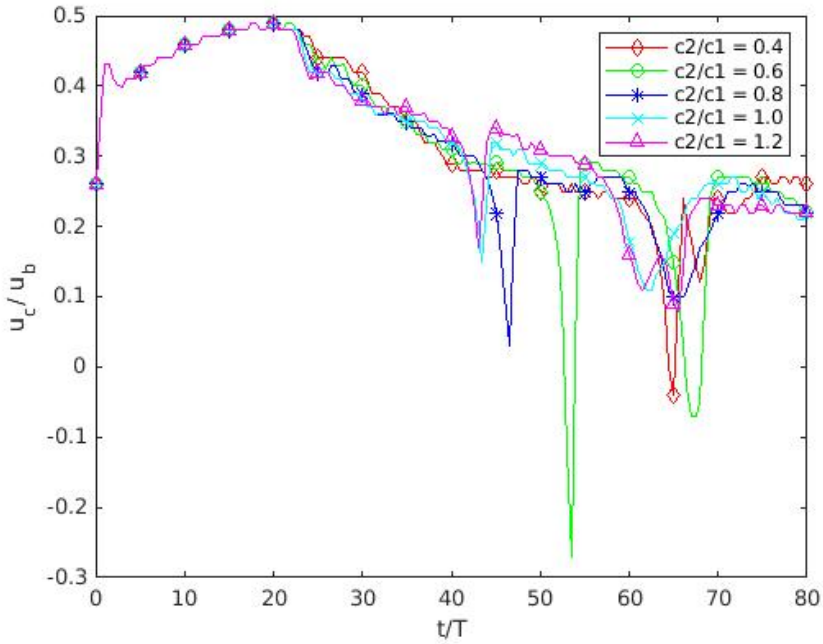

Figure 4: Horizontal velocity of the gravity current as a function of time for different density ratios.

before it hits the pynocline. For simulation times after this initial phase, the overall trend for all density ratios is that the gravity current velocity decreases as x_f increases. This reaffirms the expectation that the kinetic energy of the flow peaks when the current pierces the pynocline and then steadily decreases.

4.3 Energy Budget and Potential Energy

Analysis of the interaction between the gravity current and the ambient is conducted using energy budget components and their evolution, cf. Härtel, Meiburg, and Necker 2000 for a detailed derivation. The potential energy E_p is the sum of the contributions from the gravity current and ambient scalar fields.

$$E_p(t) = E_{p,c}(t) + E_{p,a}(t) \,, \tag{25}$$

where

$$E_{p,c}(t) = \int_\Omega y c_c \, dV \,, \; E_{p,a}(t) = \int_\Omega y c_a \, dV \,. \tag{26}$$

The total kinetic energy E_k is written as

$$E_k(t) = \int_\Omega \frac{1}{2} u_i u_i \, dV \,, \tag{27}$$

while losses due to viscous dissipation from the start of the flow up to time t are given by

$$L(t) = \int_t \epsilon(t) \, dt = - \int_t \int_\Omega \frac{2}{Re} s_{ij} s_{ij} \, dV \, dt \,, \tag{28}$$

Here $\epsilon(t)$ is the volume integral over the dissipation rate and s_{ij} denotes the rate of strain tensor. Provided that there are small vertical diffusion fluxes, energy conservation implies

$$E_{p,c} + E_{p,a} + E_k + L = cst. \tag{29}$$

The change in potential energy of the gravity current fluid as a function of time is given by

$$\Delta E_{p,c}(t) = E_{p,c}(t) - E_{p,c}(0) \,. \tag{30}$$

Similarly, the change in potential energy of the ambient fluid as a function of time is given by

$$\Delta E_{p,a}(t) = E_{p,a}(t) - E_{p,a}(0) \,. \tag{31}$$

The change in gravity current fluid potential energy normalized by the initial gravity current potential energy is analyzed for various c_2/c_1. As seen in figure 5a, as c_2/c_1 decreases, there is an associated greater loss of gravity current potential energy after $t/T = 40$. This is a result of the higher kinetic energy for lower density ratios, as shown in figure 5b. Upon release of the lock, the potential energy of the gravity current fluid is converted into kinetic energy and viscous losses accumulate. The momentum carried by the gravity current wave is higher after the simulation time of 40 for lower density ratios. As the gravity current pierces the pynocline at $t/T = 23$, a fraction of its kinetic energy is used

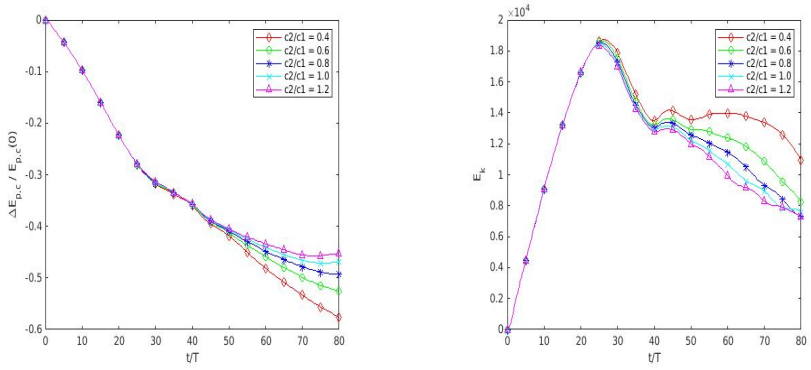

(a) Gravity current potential energy (b) Kinetic energy

Figure 5: The change in gravity current potential energy normalized by the initial gravity current potential energy and the total kinetic energy for various c_2/c_1.

to lift the ambient fluid, so that the overall kinetic energy of the flow peaks and then steadily declines. This is illustrated in figure 5b. The instantaneous viscous dissipation (figure 6a) and kinetic energy plots mirror each other in the initial portion of the flow before the gravity current hits the pynocline. This confirms the physical expectation that the viscosity of the fluid takes energy from the motion of the fluid and transforms it into internal energy of the fluid. As c_2/c_1 decreases, there is an increase in viscous dissipation $\epsilon(t)$ and cumulative viscous losses L, which is shown in figure 6.

In addition, the potential energy of the ambient fluid was analyzed for the same c_2/c_1 ratios. Figure 7a demonstrates that as c_2/c_1 increases, there is an increase in the potential energy of the ambient fluid. A larger density ratio results in a denser ambient, which has an associated higher potential energy since the ambient potential energy is a function of the ambient concentration. Once the gravity current hits the pynocline of the ambient fluid, the ambient fluid is lifted. The potential energy of the ambient for all density ratios increases as the kinetic energy of the gravity current is converted into ambient potential energy. There is a greater change in ambient potential energy as c_2/c_1 increases, as shown in figure 7b. This is a result of the the gravity current having a larger intrusion component as c_2/c_1 increases and a smaller hyperpycnal component.

The total energy of the fluid system should remain the same according to energy conservation. The total energy of the system is estimated using equation 29. A plot of the total energy as a function of time for various c_2/c_1 is shown in figure 8. The energy does not remain constant in the simulations, with the percent change for each c_2/c_1 ratio shown in table 2. The reason that this occurs is due to an overestimate of viscous losses in the system and mass loss due to the Immersed Boundary Method, which is discussed in the next section.

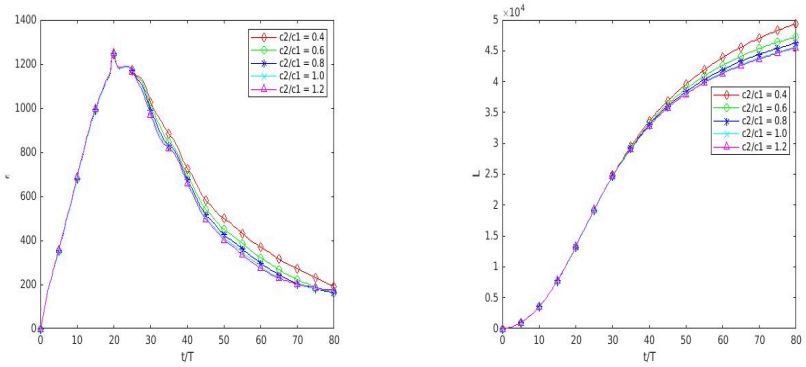

(a) Instantaneous viscous dissipation $\epsilon(t)$ (b) Cumulative viscous losses L

Figure 6: Viscous dissipation and cumulative viscous losses as a function of time for various density ratios.

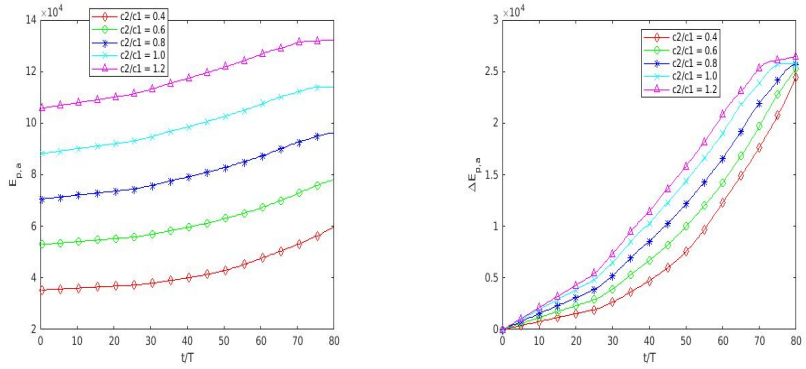

(a) Potential energy of ambient fluid (b) Change in ambient potential energy

Figure 7: Potential energy of ambient fluid for various c_2/c_1.

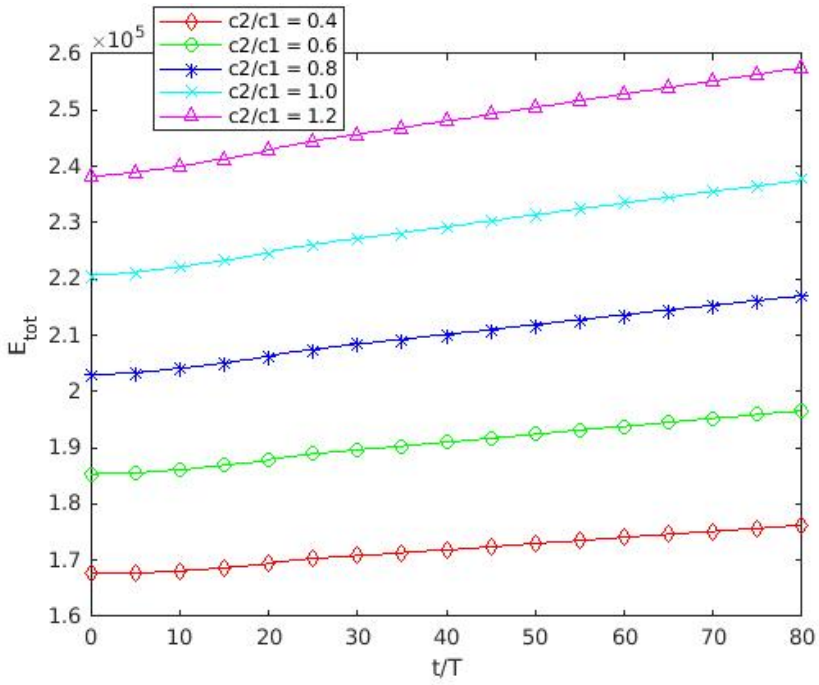

Figure 8: Total energy of the entire fluid volume for various c_2/c_1.

Sim.	c_2/c_1	Percent change in total energy
1	0.4	5.06
2	0.6	6.04
3	0.8	6.90
4	1.0	7.69
5	1.2	8.11

Table 2: Percent change in the total energy for various c_2/c_1.

4.4 Mass Loss due to IBM

The mass of gravity current fluid is defined as

$$m = \int_{\Omega} c_c \, dV \, . \tag{32}$$

where Ω represents the total fluid volume. A Matlab script is utilized to ensure that the concentration points within the solid region of the slope are specified as zero. Otherwise, an unphysical phenomena occurs wherein the mass of the entire volume increases, which violates conservation of mass. An analysis of the mass loss due to the Immersed Boundary Method (IBM) is shown in figure

9. As the density ratio is increased, the relative mass loss increases past the simulation time of $t/T = 23$. This larger mass loss results in a higher percent error with the change in total energy. A snapshot of the gravity current fluid concentration at this time is shown in figure 10. The mass loss approaches zero when the head of the gravity current is its fullest and this occurs right before the head of the gravity current splits. This occurs for all density ratios because the initial gravity current wave concentration c_1 is the same for all simulations.

5 Summary

The simulations provide key insights into the physics of gravity current flow down an incline. The effect of various density ratios c_2/c_1 on several flow parameters is shown. When the gravity current is lighter than the lower layer ($c_2/c_1 > 1$), then the gravity current intrudes at the pynocline with no hyperpycnal component. This is clearly shown in the subplot for density ratio ($c_2/c_1 = 1.2$) at the simulation time $t/T = 60$. When the gravity current is heavier than the lower layer ($c_2/c_1 < 1$), then the gravity current splits into an intrusion at the pynocline and a hyperpycnal bottom current that continues to move down the slope. This hyperpycnal component is most evident in the subplot for the density ratio $c_2/c_1 = 0.4$ at $t/T = 60$. As c_2/c_1 increases, the gravity current is more dominated by the intrusion component and less by the hyperpycnal component. As the simulation progresses, the x-direction gravity current front location x_f increases because the gravity current is moving further down the slope. There is no clear correlation between the density ratio and x_f location. The density ratio also has a clear effect on the y-direction gravity current location y_f for later times. Lower density ratios result in gravity currents that descend lower before moving upwards. This reaffirms the physical expectation that the hyperpycnal component of the gravity current descends beneath the lower layer for $c_2/c_1 < 1$. For higher density ratios, there is still oscillatory movement in the wave, but the motion is more horizontal, just above the pynocline $h_p = 1.0$. This confirms the expectation that the gravity current will intrude at the pynocline for $c_2/c_1 > 1$. The gravity current velocity increases for all density ratios during the initial period before it hits the pynocline. For simulation times after this initial phase, the overall trend for all density ratios is that the gravity current velocity decreases as x_f increases. This reaffirms the expectation that the kinetic energy of the flow peaks when the current pierces the pynocline and then steadily decreases.

The effect of the density ratio on the energy components is analyzed. As c_2/c_1 decreases, there is an associated greater loss of gravity current potential energy after $t/T = 40$. This is a result of the higher kinetic energy for lower density ratios. Upon release of the lock, the potential energy of the gravity current fluid is converted into kinetic energy and viscous losses accumulate. The momentum carried by the gravity current wave is higher after the simulation time of 40 for lower density ratios. As the gravity current pierces the pynocline at $t/T = 23$, a fraction of its kinetic energy is used to lift the ambient fluid, so

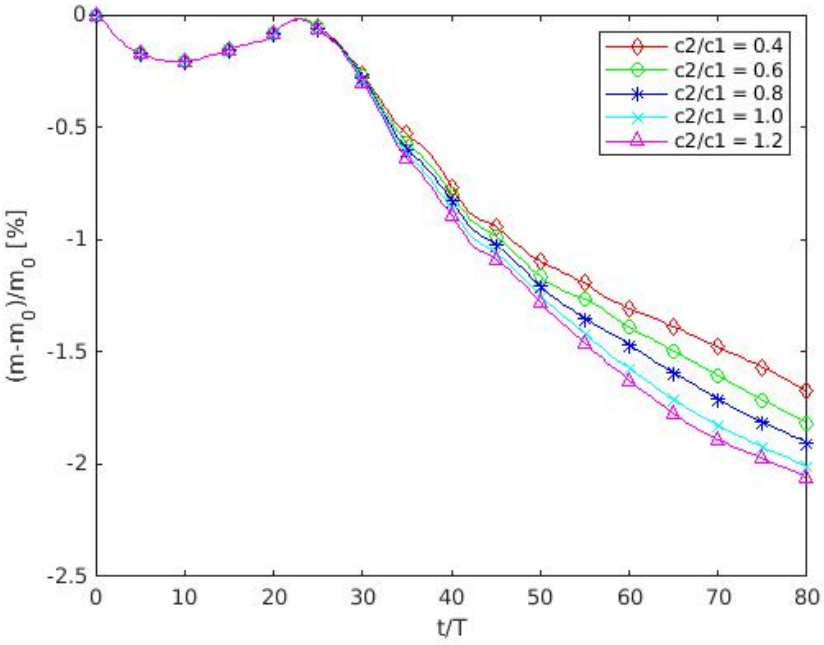

Figure 9: Relative change of mass of gravity current fluid in the entire volume as a function of time for various initial concentration ratios c_2/c_1.

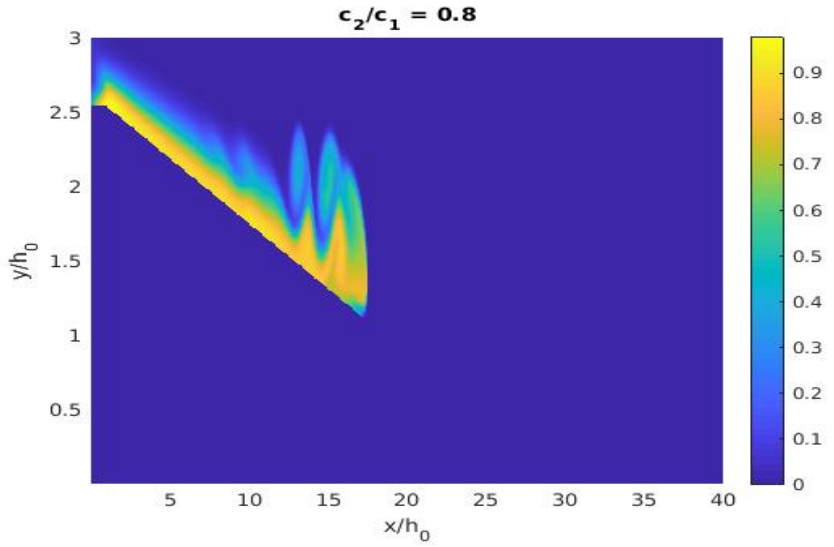

Figure 10: Snapshot of the gravity current fluid concentration c_c at $t/T = 23$.

that the overall kinetic energy of the flow peaks and then steadily declines. The instantaneous viscous dissipation and kinetic energy plots both increase rapidly in the initial portion of the flow before the gravity current hits the pynocline. This affirms the physical expectation that the viscosity of the fluid takes energy from the motion of the fluid and transforms it into internal energy of the fluid. As c_2/c_1 decreases, there is an increase in viscous dissipation $\epsilon(t)$ and cumulative viscous losses L. As c_2/c_1 increases, there is an increase in the potential energy of the ambient fluid. A larger density ratio results in a denser ambient, which has an associated higher potential energy since the ambient potential energy is a function of the ambient concentration. Once the gravity current hits the pynocline of the ambient fluid, the ambient fluid is lifted. The potential energy of the ambient for all density ratios increases as the kinetic energy of the gravity current is converted into ambient potential energy. There is a greater change in ambient potential energy (equation 31) as c_2/c_1 increases. This is a result of the the gravity current having a larger intrusion component as c_2/c_1 increases and a smaller hyperpycnal component. The total energy of the system should remain constant by energy conservation. In the simulations, the total energy increases slightly, with a maximum increase of 8.1% for simulation 5. The reason that this occurs is due to an overestimate of viscous losses in the system and the mass loss due to the immersed boundary method. As the density ratio is increased, the relative mass loss of the gravity current increases in magnitude past the simulation time of $t/T = 23$. This larger mass loss results in a higher percent error with the change in total energy.

The author would like to thank R. Ouillon and T. Kollner for their assistance on the project, particularly in learning how to run the code and to understand the physical problem. The author would also like to thank Professor Meiburg for providing the resources necessary to complete the project and his guidance whenever any issues were encountered. Computational resources for this work used the Extreme Science and Engineering Discovery Environment (XSEDE), which was supported by the National Science Foundation.

References

Ascher, U. M. and L. R. Petzold (1998). *Computer Methods for Ordinary Differential Equations and Differential-Algebraic Equations*. Society for Industrial and Applied Mathematics.

Bennett, Ted D. (2012). *Transport by Advection and Diffusion. Momentum, Heat, and Mass Transfer*. Wiley.

Ferziger, J.H. and M. Perić (2002). *Computational Methods for Fluid Dynamics*. 3rd. Springer-Verlag Berlin Heidelberg.

Fletcher, C. A. J. (1991). *Computational Techniques for Fluid Dynamics 2. Specific Techniques for Different Flow Categories*. Second. Springer-Verlag Berlin Heidelberg.

Härtel, C., E. Meiburg, and F. Necker (2000). "Analysis and direct numerical simulation of the flow at a gravity current head. Part 1. Flow topology and front speed for slip and no-slip boundaries". In: *Journal of Fluid Mechanics* 418.

Hogg, Charlie A. R. et al. (2018). "Shoaling internal waves may reduce gravity current transport". In: *Environmental Fluid Mechanics* 18.2, pp. 383–394.

M.M., Nasr-Azadani, and E. Meiburg (2011). "TURBINS: An immersed boundary, Navier-Stokes code for the simulation of gravity and turbidity currents interacting with complex topographies". In: *Computers Fluids* 45, pp. 14–28.

Spalart, Philippe R., Robert D. Moser, and Michael M. Rogers (1990). "Spectral Methods for the Navier-Stokes Equations with One Infinite and Two Periodic Directions". In: *Journal of Computational Physics* 96, pp. 297–324.

Sutherland, B. R. (2010). *Internal Gravity Waves*. Cambridge: Cambridge University Press.

Ungarish, M. (2009). *An introduction to gravity currents and intrusions*. Chapman and Hall/CRC.